**To cite this article:** LEI Z Y, WANG C X, WU C J, et al. Underwater online dynamic strain test of CFRP propeller with embedded FBG sensors [J/OL]. Chinese Journal of Ship Research, 2022, 17(2). http://www.ship-research.com/en/article/doi/10.19693/j.issn.1673-3185.02323.

**DOI:** 10.19693/j.issn.1673-3185. 02323

# Underwater online dynamic strain test of CFRP propeller with embedded FBG sensors

*LEI Zhiyang*[1,2], *WANG Chunxu*[1,2], *WU Chongjian*[1,2], *DING Guoping*[*3], *YAN Xiaoyu*[3]

1 China Ship Development and Design Center, Wuhan 430064, China;

2 National Key Laboratory on Ship Vibration and Noise, Wuhan 430064, China;

3 School of Mechanical and Electronic Engineering, Wuhan University of Technology, Wuhan 430070, China

**Abstract:** [**Objective**] The carbon fiber reinforced plastic (CFRP) propeller has such advantages as light weight, high strength, low vibration, low noise, corrosion resistance, and fatigue resistance. To accurately ascertain the deformation and strain of CFRP propeller blades under hydrodynamic load, this paper proposes an online measurement method for the dynamic strain of CFRP propellers under submerged operation conditions. [**Method**] Fiber Bragg grating (FBG) sensors are embedded in a CFRP propeller, and an underwater dynamic strain test system is built. Two types of test conditions are set: (1) the velocity is 0 m/s, and the rotation speed increases from 50 to 400 r/min; (2) the rotation speed is 427 r/min, and the velocity increases from 0 to 1.6 m/s. The dynamic strain data of the CFRP propeller under the above conditions is obtained by the FBG sensors and analyzed in the time and spectrum domains. [**Results**] The results show that the dynamic strain frequencies of each FBG sensor on the CFRP propeller are the same and related to the rotation speed, while the dynamic strain amplitude of each FBG sensor has no obvious relationship with the rotation speed or velocity, but depends on the position of the sensor, which reflects the mechanical characteristics of the propeller structure. [**Conclusion**] The underwater online dynamic strain test of the CFRP propeller is realized, and test results are reasonable and reliable. This provides an important empirical basis for the theoretical design and analysis of the CFRP propeller, which is of great significance for the study of its vibration noise and hydrodynamic performance.

**Key words:** embedded fiber Bragg grating (FBG) sensors; carbon fiber reinforced plastic (CFRP) propeller; dynamic strain; underwater online test

**CLC number:** U664.33

## 0 Introduction

Marine metal propellers are plagued by problems such as corrosion and fatigue life. Carbon fiber reinforced plastic (CFRP) has the advantages of light weight, high strength, corrosion resistance, fatigue resistance, and designability [1-2], which has become a new enabler for better performance of marine propellers and drawn broad attention.

CFRP propellers are distinguished from their metal counterparts most in that the blades made from composite materials generate adaptive bending and torsional deformation according to hydrodynamic load [3-4]. The anisotropy and bending-torsional coupling of composite materials cause the change of propeller pitch, which enables superior hydrodynamic performance of CFRP propellers to those of metal ones in a non-uniform flow field. In addition,

**Received:** 2021－03－18 **Accepted:** 2021－05－22

**Supported by**: National Natural Science Foundation of China (51775400)

**Authors:** LEI Zhiyang, male, born in 1990, Ph.D.
WANG Chunxu, male, born in 1990, Ph.D.
WU Chongjian, male, born in 1960, Ph.D.
DING Guoping, female, born in 1979, Ph.D., professor, Research interest: optical fiber sensing test.

***Corresponding author:** DING Guoping

the large damping of CFRP propellers helps reduce their vibration and noise. For the sake of the performance evaluation of a CFRP propeller, accurate tests for obtaining its blade deformation, dynamic strain, and vibration are of vital importance to the research and design of such propellers.

As conventional sensing technology faces the problems concerning underwater insulation, flow field interference, and signal transmission, measuring the operational deflection shape and dynamic strain of propellers in underwater operation has always been an engineering challenge. The common strain measurement method is to arrange strain gauges on the surface of the propeller to be investigated. However, due to its underwater operation, the sizes and weights of conventional strain gauges and transmission cables greatly influence the surface flow field and hydrodynamic performance of the propeller. Moreover, previous studies have suggested that pasting strain gauges on the surface of blades can aggravate the cavitation effect [4].

As a new type of optical sensor, fiber Bragg grating (FBG) sensor realizes the absolute measurement of the strain or temperature of the object through the wavelength shift of the grating. Optical fiber sensing features small size, light weight, the availability of multi-point measurement with one fiber, electromagnetic interference resistance, and stable underwater signal transmission which are not possessed by the conventional optical imaging method and electrical method [5-6]. Thus, the test methods for underwater operational deflection shape and strain of propellers based on optical fiber sensing have been studied and gained attention.

Zetterlind et al. [7] first analyzed the feasibility of the strain measurement by embedding FBG sensors in the composite propeller blades. Subsequently, Zetterlind et al. [8] monitored the static and dynamic strain of composite propeller blades under constant axial load and cyclic bending load in air by employing an extrinsic Fabry-Perot interferometer (EFPI). In this way, they verified the applicability of optical fiber sensors in the fatigue tests on composite propellers. Wozniak [9] monitored the strain of composite propeller blades with embedded FBG sensors and discussed the design and technique regarding how to lead the optical fiber out of the composite material. Herath et al. [10] measured the strain of composite blades by pasting FBG sensor arrays on their surface. Javdani et al. [11] used FBG sensor arrays to test the vibration of the blade specimens of a cantilevered steel propeller. In addition, they further studied the vibration characteristics of propellers in air and underwater [12] by installing an FBG sensor array on the full-size steel propeller blade. The above research explored and verified the feasibility and applicability of FBG sensing technology in the static strain test on composite and steel propellers in air, but less involved real-time online dynamic strain test on the blades of CFRP propellers in underwater operation.

This paper proposes embedding FBG sensors in a CFRP propeller to achieve the online dynamic strain test on the blades in underwater operation. We prepared the CFRP propeller with embedded FBG sensors and build a real-time underwater online dynamic strain test system for CFRP propellers. Dynamic strain tests were conducted on the blades of the CFRP propeller in underwater operation under various operating conditions, so as to make clear the dynamic strain characteristics of composite propellers in underwater operation. This research provides test support for the study and design optimization of fluid-solid interaction and hydrodynamic performance.

## 1 CFRP propeller structure

The CFRP propeller with embedded FBG sensors in this paper has a split metal embedded part-blade structure. It can be divided into three parts, i.e., metal hub, metal embedded parts (five pieces), and CFRP blades (five pieces), the structure of which is presented in Fig. 1.

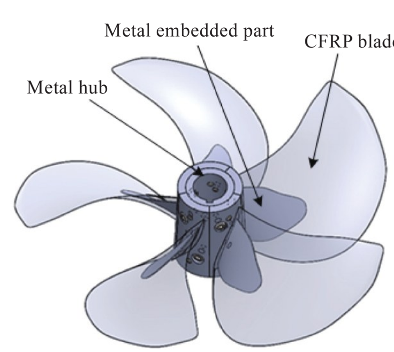


Fig. 1 Metal-CFRP blade

In this structure, the metal embedded parts and the CFRP blades are solidified into an integral whole (metal-CFRP blades) via compression molding and then connected with the metal hub through screws and pins. As the five metal-CFRP blades of such structure are manufactured separately, if one is damaged, replacing it is convenient, which thus reduces the maintenance cost. The FAW200RC36

(T700 Series) unidirectional carbon fiber prepreg of Zhongfu Shenying Carbon Fiber Co., Ltd. was selected as the material of the CFRP propeller. The main structural parameters of the propeller are listed in Table 1.

**Table 1 Main parameters of CFRP propeller**

| Parameter | Value |
|---|---|
| Propeller diameter/mm | 240 |
| Number of blades | 5 |
| Hub diameter ratio | 0.175 |
| Disc ratio | 0.8 |
| Blade tilt angle/(°) | 24.50 |
| Total trim angle of blade/(°) | 8 |

## 2 CFRP propeller with embedded FBG sensors

### 2.1 Sensing principle and multiplexing technology of FBG

The sensing principle of FBG sensors is presented in Fig. 2. The incident light is broadband light with various wavelengths. Upon its incidence on the grating area, only the light waves of specific wavelengths are reflected, while those of other wavelengths keep propagating along the fiber directly through the grating without being influenced. The wavelength of the reflected light is known as the Bragg wavelength, with its expression shown below:

$$\lambda_B = 2n_{eff}\Lambda \tag{1}$$

where $\lambda_B$ represents the reflection wavelength of FBG, $\Lambda$ the grating period, and $n_{eff}$ the effective refractive index of the grating. The factors determining the reflection wavelength of the grating mainly involve $\Lambda$ and $n_{eff}$. When an FBG sensor reports a change in the axial strain of the grating due to the deformation of the grating area under external force, the $\Lambda$ and $n_{eff}$ also change accordingly, which results in a $\lambda_B$ variation. When the temperature of the grating changes, the optical fiber material generates strain amid the thermal expansion or contraction, which brings about the change of $\lambda_B$. Meanwhile, the thermo-optic effect also changes $n_{eff}$ and thus alters $\lambda_B$.

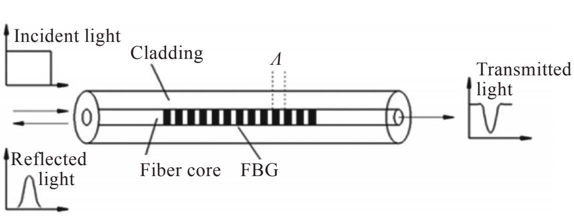


Fig. 2 FBG sensing principle

It is known from Equation (1) that the shift of the center wavelength of the FBG can be expressed as

$$\Delta\lambda_B = 2\Delta n_{eff}\Lambda + 2n_{eff}\Delta\Lambda \tag{2}$$

In light of the theories of elasticity, elasto-optical effect, thermo-optic effect, and thermal expansion effect, Equation (2) can be rewritten as

$$\Delta\lambda_B = \lambda_{B0}(\alpha+\xi)\Delta T + \lambda_{B0}(1-P_e)\varepsilon \tag{3}$$

where $\Delta T$ is the temperature change of the FBG; $\alpha$ is the thermal expansion coefficient of the optical fiber; $\xi$ is the thermo-optic coefficient; $\lambda_{B0}$ is the initial wavelength; $\varepsilon$ is the strain variation of the FBG; $P_e$ is the effective elasto-optic coefficient. The grating used in this paper is made of quartz, so $P_e$ = 0.22.

When an FBG sensor is in a constant temperature field, i.e., $\Delta T = 0$, one can obtain

$$\Delta\lambda_B = \lambda_{B0}(1-P_e)\varepsilon = K_\varepsilon\varepsilon \tag{4}$$

where $K_\varepsilon$ represents the strain sensitivity of the FBG sensor. As indicated by Equation (4), at constant external temperature, the shift of the center wavelength of the reflection spectrum is only influenced by the changes in the stress field where the FBG sensor is located. Under the effect of external stress field, the grating changes $\Lambda$ and $n_{eff}$, thus bringing about the variations of the reflection wavelength and reflection spectrum of the FBG. Therefore, we can have the corresponding information on stress and strain by monitoring $\Delta\lambda_B$. This is the basic principle of stress and strain monitoring through FBG. Under the same conditions, as the transverse sensitivity of the FBG is much smaller than the longitudinal sensitivity, we merely take into account the longitudinal strain of the sensor in practical application generally, which thus leads to the mere use of FBG to measure the longitudinal strain.

As shown in Fig. 3, wavelength-division multiplexing is one of the most significant advantages of FBG sensors. It involves writing multiple gratings on one fiber. An independent and specific wavelength interval within the available scope of the demodulator or spectrometer is assigned to each grating whose reflection peak varies with the measured change within the wavelength range. We adopt a set of demodulation devices to detect the composite spectrum formed by the reflection spectra of all gratings, so as to obtain the shift of the center wavelength of each grating from each independent wavelength interval assigned in advance. In this way, we enable massive distributed multi-grating measure-

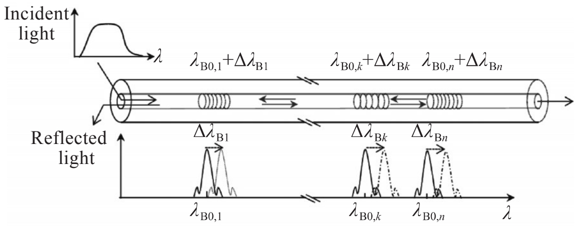


Fig. 3 FBG wavelength-division multiplexing principle

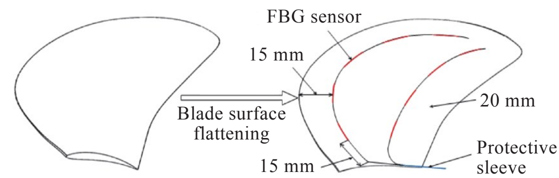


Fig. 4 Schematic diagram of the position of the FBG sensor in the blade

ment with one fiber.

## 2.2 Layout of embedded FBG sensors

The position layout of embedded FBG sensors mainly takes into account the layer thickness and strain distribution of the blades. The diameter of the FBG sensor is 0.125 mm. When it is embedded between the layers of CFRP blades, the thickness of the layer at the sensor should be more than 10 times its diameter in order to avoid delamination and cracking. Besides, the FBG sensor should be arranged in the area featuring significant strain changes. According to the above considerations, we determine the position of the FBG sensor in the blade, as shown in Fig. 4.

According to the embedding position and strain measurement range of the FBG sensor, we customized two groups of FBG sensors in series (FBG1 and FBG2). The Nos., center wavelengths, and distance of the sensors are presented in Fig. 5. Each sensor is distinguished via wavelength-division multiplexing.

The surface and back of the CFRP propeller blade present the same layer form. The angle of single-side layer is $[0°_2/45°_2/0°_2/45°_2/0°_2]$ from the blade surface inward, where "$X°_2$" represents that the fiber is laid at an angle of X° for two layers continuously. The layer No. ranges from 1 to 10, with the FBG sensors embedded between the 8th and 9th layers of the blades.

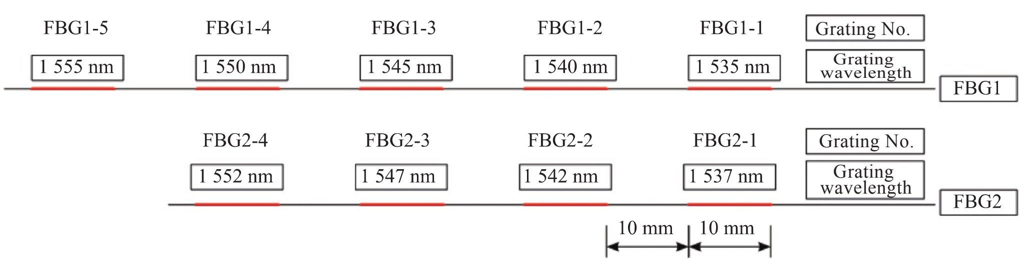


Fig. 5 Center wavelengths and distance of FBG sensors

## 2.3 Fabrication of CFRP propeller

The CFRP propeller with embedded FBG sensors was fabricated by compression molding. The formed CFRP propeller with embedded FBG sensors is shown in Fig. 6.

Fig. 6 CFRP propeller with embedded FBG sensors

# 3 Underwater dynamic strain test

## 3.1 Underwater dynamic strain test system for CFRP propeller

The underwater dynamic strain test on the CFRP propeller was conducted in the towing tank of Wuhan University of Technology, where the propeller was driven to rotate and move forward by the towing waterwheel. Therefore, we designed the underwater dynamic strain test system for the CFRP propeller according to the structure of the towing waterwheel. As shown in Fig. 7, the structure of the test system is mainly composed of towing waterwheel, CFRP propeller with embedded FBG sensors, fiber-optic slip ring, fixed end of rotor, fixed end of stator, fixed support of stator, and FBG wavelength demodulator. The CFRP propeller is installed on the rotating shaft of the towing waterwheel. The tail end of the propeller is equipped with a fiber-optic slip ring, whose rotor is installed at the fixed end of the rotor and then connected with the tail end of the propeller through threads, so that the rotor of the slip ring is enabled to rotate with the propeller. The fixed end of stator is used for the installation of the stator of fiber-optic slip ring, which is connected with the towing waterwheel through the fixed support. The optical fiber is led to the FBG demodulator that is placed on the bank of the tank.

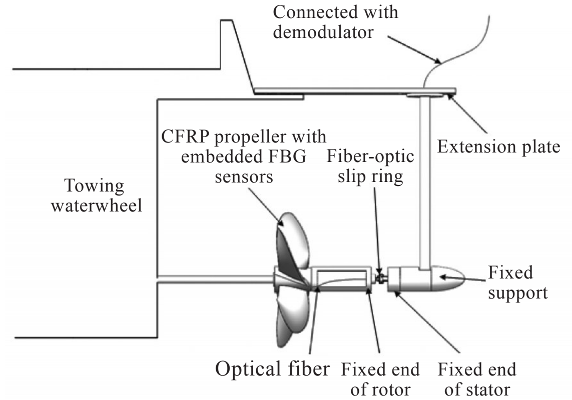


Fig. 7 Schematic diagram of underwater dynamic strain test system for CFRP propeller

According to the schematic diagram of the test system shown in Fig. 7, we install the CFRP propeller with embedded FBG sensors, fixed end of rotor, fiber-optic slip ring, fixed end of stator, and fixed support on the towing waterwheel in sequence. Then we conduct fusion welding of the embedded FBG sensors and the optical fiber at the rotor end of the fiber-optic slip ring and connect the optical fiber at the stator end to the demodulator. We also detect whether the optical fiber signal is normal during the installation. As the fiber-optic slip ring is a single-channel slip ring, we connected one string of FBG sensors in series (FBG2) with the fiber-optic slip ring and transmit the sensor signal to the demodulator.

In the efforts to build the underwater dynamic strain test system, it is necessary to ensure the coaxiality among the fixed end of rotor, the fiber-optic slip ring, and the fixed end of stator, because the rotor end and the propeller are coaxial and at the same rotation speed during the test. Any excessive deviation in the installation and matching between the fixed end of rotor and that of stator leaves the slip ring prone to damage during operation. Accordingly, in the building of the test system, it is required to adjust the position and angle of the fixed end of stator and detect whether the optical fiber signal performs well before carrying out the relevant test. Fig. 8 presents the built underwater dynamic strain test system for the CFRP propeller.

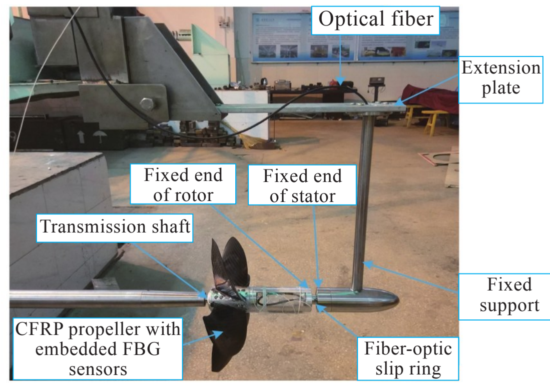


Fig. 8 Underwater dynamic strain test system for CFRP propeller

## 3.2 Underwater online dynamic strain test on CFRP propeller

When the propeller is in underwater operation, its rotation speed and velocity are two important parameters influencing its hydrodynamic performance. Accordingly, this paper set two types of test conditions (varying rotation speed or velocity) to study the dynamic strain characteristics of the CFRP propeller in underwater operation. The test site is shown in Fig. 9.

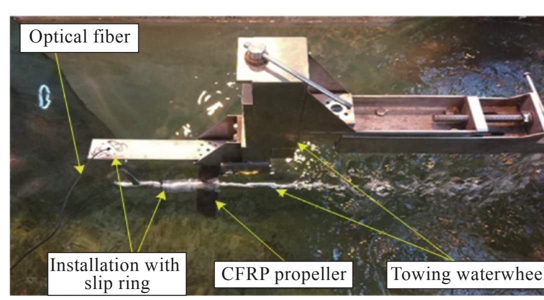


Fig. 9 Underwater online dynamic strain test on CFRP propeller

The specific test conditions were set as follows:

1) Test condition 1. The velocity of the propeller was 0 m/s, and eight rotation speeds were tested, including 50, 100, 150, …, 400 r/min, an increase of 50 r/min in turn. After the condition became stable at each rotation speed, we collected the data of the embedded FBG sensors. The sampling frequency of the FBG wavelength demodulator was set at 2 kHz.

2) Test condition 2. The rotation speed of the propeller was set at 427 r/min. The data collection under this condition involved two stages. At the

velocity of 0, 0.2, 0.4, …, 1.6 m/s (nine kinds), an increase of 0.2 m/s in turn: After the test condition became stable at each velocity, we collected the data of the embedded FBG sensors and the hydrodynamic data of the CFRP propeller. At the velocity of 1.8, 2.0, 2.2, 2.4, 2.6, and 2.8 m/s, we merely collected the hydrodynamic data of the CFRP propeller due to the noise interference of the test system.

## 3.3 Test results and analysis

### 3.3.1 Test condition 1

Figs. 10 (a) and 10 (b) present the strain curves of the embedded FBG sensors in the time domain at the rotation speeds of 50 and 400 r/min in test condition 1, which are featured by remarkable periodicity. By use of Fourier transform and Hanning window, we obtain the spectra of the dynamic strain (Figs. 10 (c) and 10 (d)) *APF* in the figures represents the shaft frequency of the propeller rotation, which is calculated by dividing the rotation speed by 60, and $r$ is the rotation speed. Since the strain curves in the time and spectrum domains at other rotation speeds in test condition 1 are similar to those at 50 and 400 r/min, there is no more detailed description of them here.

The spectra of dynamic strain in Fig. 10 indicate

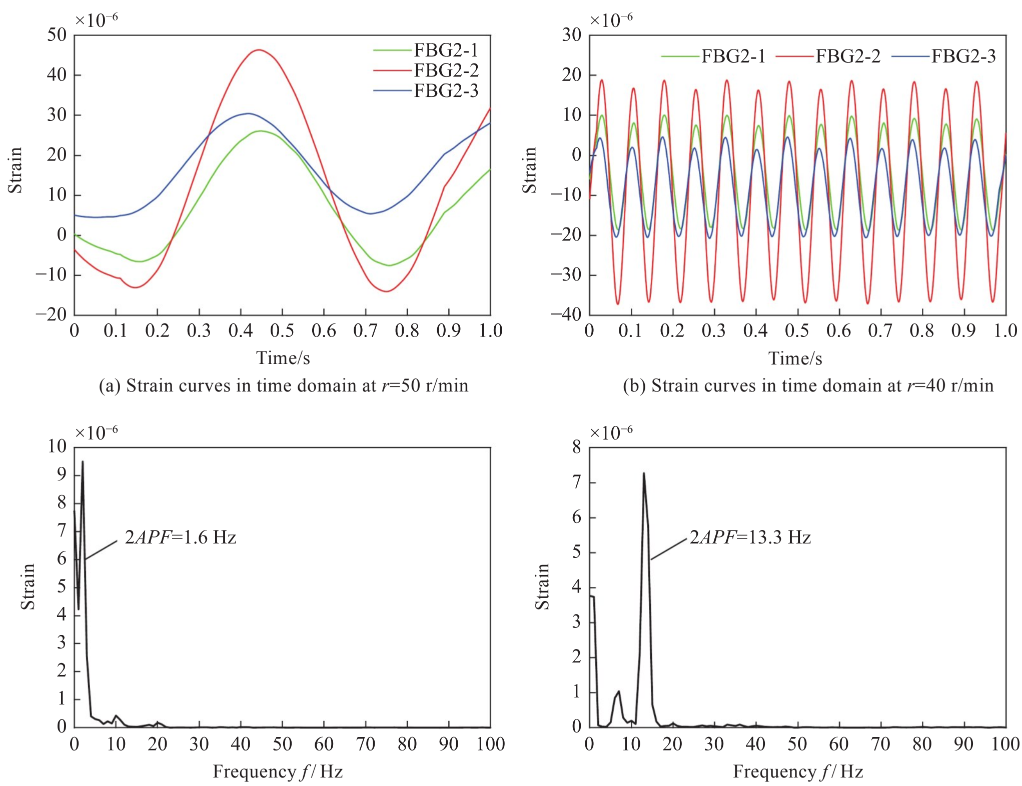


(a) Strain curves in time domain at $r$=50 r/min

(b) Strain curves in time domain at $r$=40 r/min

(c) Strain spectrum of FBG2-1 at $r$=50 r/min

(d) Strain spectrum of FBG2-1 at $r$=400 r/min

Fig. 10 Strain curves of embedded FBG sensors at different rotation speeds

that the signal-to-noise ratios of the test results are high and there are obvious peaks at specific frequencies. Table 2 lists the characteristic frequency and amplitude of the strain of each FBG sensor at each rotation speed.

The results presented in Table 2 show that the characteristic frequency of the strain of each FBG sensor is two times the *APF*. This may result from the unevenness of incoming flow and the misalignment of the propeller and the shaft due to the influence of the support of the test system. We analyze the amplitudes of the dynamic strain of the FBG sensors. At different rotation speeds, the amplitudes of the strain of the three FBG sensors are in the same order, namely that FBG2-2 has the largest amplitude while FBG2-3 has the smallest. This suggests the largest strain and deformation occur at the position of FBG2-2, and the smallest strain and deformation can be found near FBG2-3. This manifests that when the propeller operates underwater, the strain and deformation vary at different positions of the blades, which depends on the mechanical characteristics of the propeller structure.

**Table 2 Frequencies and amplitudes of strain at different rotation speeds**

| $r$/(r·min$^{-1}$) | *APF*/Hz | Characteristic frequency of strain/Hz | | | Amplitude of strain/$10^{-6}$ | | |
|---|---|---|---|---|---|---|---|
| | | FBG2-1 | FBG2-2 | FBG2-3 | FBG2-1 | FBG2-2 | FBG2-3 |
| 50 | 0.833 | 1.636 | 1.636 | 1.636 | 9.450 | 17.170 | 7.011 |
| 100 | 1.667 | 3.339 | 3.339 | 3.339 | 9.121 | 16.046 | 6.564 |
| 150 | 2.500 | 4.968 | 4.968 | 4.968 | 10.096 | 17.974 | 7.205 |
| 200 | 3.333 | 6.645 | 6.645 | 6.645 | 9.063 | 15.140 | 6.557 |
| 250 | 4.167 | 8.333 | 8.333 | 8.333 | 8.823 | 14.213 | 6.367 |
| 300 | 5.000 | 10.05 | 10.05 | 10.05 | 10.196 | 17.080 | 7.962 |
| 350 | 5.833 | 11.66 | 11.66 | 11.66 | 10.084 | 17.067 | 7.833 |
| 400 | 6.667 | 13.33 | 13.33 | 13.33 | 7.206 | 14.018 | 7.104 |

### 3.3.2 Test condition 2

Fig. 11 shows the strain curves of the FBG sensors in the time and spectrum domains at the rotation speed $r$ of 427 r/min and the velocities $v$ of 0.2 and 1.6 m/s. The strain curves in the domains at other velocities in test condition 2 are similar to those at $v$ = 0.2 and 1.6 m/s, so there is no more detailed description of them here. Table 3 lists the characteristic frequency and amplitude of the strain of each FBG sensor at each velocity.

The results in Table 3 show that when the rotation speed is constant, the characteristic frequencies of dynamic strain of the three FBG sensors remain unchanged at 14.2 Hz at various velocities, which is still two times the *APF*. Among the dynamic strain amplitudes collected by the three FBG sensors, the value reported by FBG2-2 remains the largest and that reported by FBG2-3 the smallest, which is consistent with the test results in test condition 1.

In test condition 2, when the velocity is 0−1.6 m/s, we collect the dynamic strain data of the FBG sensors and hydrodynamic data of the propeller simultaneously; when the velocity is greater than 1.6 m/s, we collect only the hydrodynamic data of the propeller. We draw the open water diagram of the CFRP propeller at a velocity of 0−2.8 m/s, as shown in Fig. 12, where $K_T$ is the thrust coefficient, $K_Q$ the torque coefficient, and $\eta$ the propeller effi-

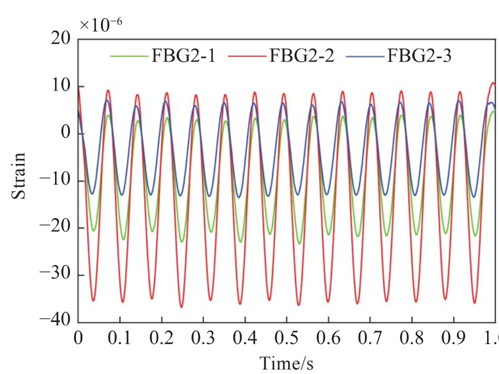


(a) Strain curves in time domain at $v$=0.2 m/s

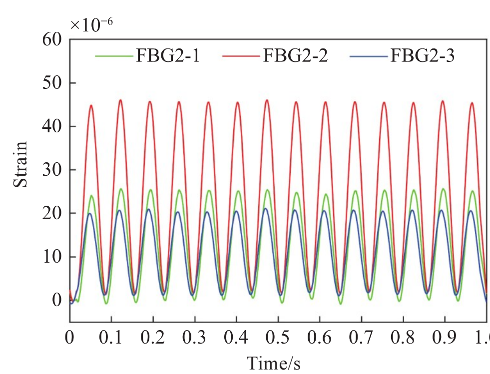


(b) Strain curves in time domain at $v$=1.6 m/s

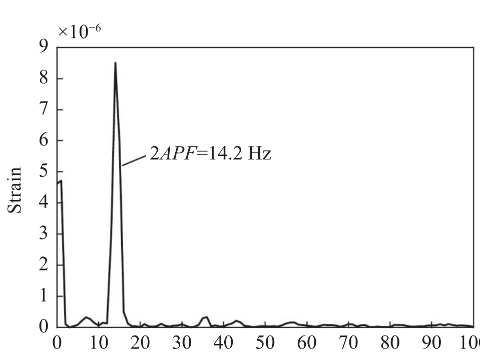


(c) Strain spectrum at $v$=0.2 m/s

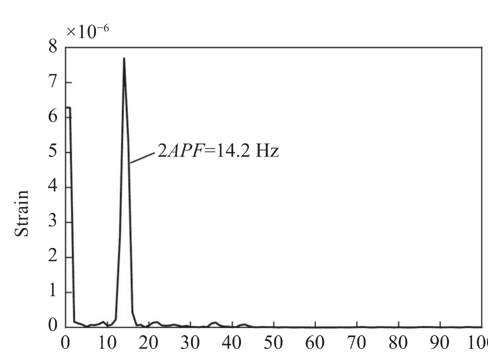


(d) Strain spectrum at $v$=1.6 m/s

Fig. 11 Strain curves of embedded FBG sensors at different velocities

**Table 3 Frequencies and amplitudes of strain at different velocities**

| $v$/（m·s$^{-1}$） | Characteristic frequency of strain/Hz | | | Amplitude of strain/$10^{-6}$ | | |
|---|---|---|---|---|---|---|
| | FBG2-1 | FBG2-2 | FBG2-3 | FBG2-1 | FBG2-2 | FBG2-3 |
| 0 | 14.2 | 14.2 | 14.2 | 7.124 | 12.93 | 6.734 |
| 0.2 | 14.2 | 14.2 | 14.2 | 8.513 | 12.52 | 6.822 |
| 0.4 | 14.2 | 14.2 | 14.2 | 8.485 | 13.50 | 6.736 |
| 0.6 | 14.2 | 14.2 | 14.2 | 8.218 | 12.66 | 6.669 |
| 0.8 | 14.2 | 14.2 | 14.2 | 7.856 | 13.74 | 6.811 |
| 1.0 | 14.2 | 14.2 | 14.2 | 7.794 | 13.06 | 6.595 |
| 1.2 | 14.2 | 14.2 | 14.2 | 8.752 | 13.14 | 6.585 |
| 1.4 | 14.2 | 14.2 | 14.2 | 8.56 | 13.17 | 6.760 |
| 1.6 | 14.2 | 14.2 | 14.2 | 7.841 | 12.05 | 6.835 |

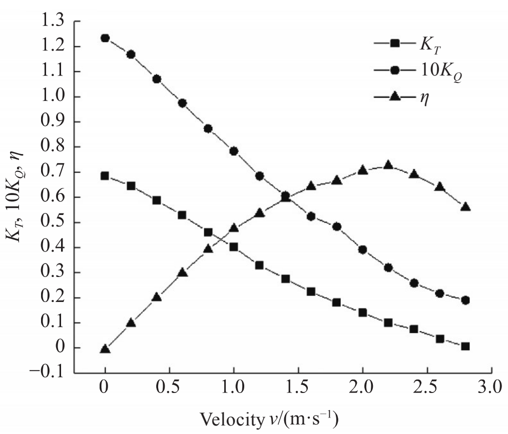


Fig. 12 Open water diagram of CFRP propeller ($n$ = 427 r/min)

ciency.

Fig. 13 presents the comparison of open water characteristics between the CFRP propeller and metal propeller with the same offsets. They have basically the same trend, which suggests that the CFRP propeller with embedded FBG sensors fulfills its basic performance and also proves the feasibility and reliability of the dynamic strain test on FBG sensors.

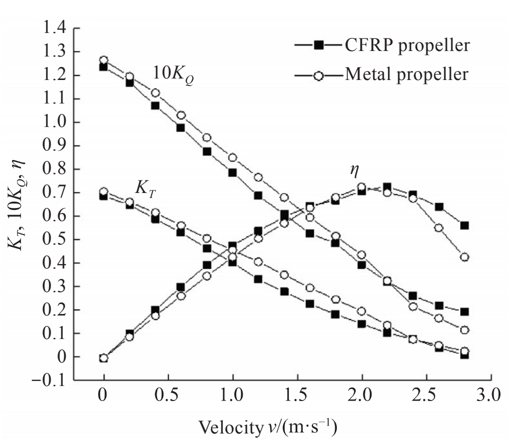


Fig. 13 Comparison of open water characteristics between CFRP propeller and metal propeller

# 4 Conclusions

Drawing on the technical advantages of FBG sensing, this paper proposes embedding FBG sensors in a CFRP propeller and builds an underwater online underwater dynamic test system for the CFRP propeller based on FBG sensors. Two kinds of test conditions are set: the velocity is 0 m/s, and the rotation speed increases from 50 to 400 r/min; the rotation speed remains unchanged at 427 r/min, and the velocity increases from 0 to 1.6 m/s. We collect the dynamic strain data of the CFRP propeller under the above two test conditions by use of FBG sensors and make the time domain and frequency domain analyses. The results show that the characteristic frequencies of dynamic strain are consistent at different measuring points on the CFRP propeller. The characteristic frequencies are mainly two times the shaft frequency, which may be caused by the unevenness in the propeller test system. The amplitude of dynamic strain at each measuring point depends on its position, namely the mechanical characteristics of the propeller structure.

This paper achieves the online dynamic strain test on the CFRP propeller in underwater operation. It verifies the feasibility of underwater dynamic strain tests on propellers and conquers the challenge of underwater online tests on propellers. The test results are reasonable and reliable. Thus, they can serve as an important empirical basis for the theoretical design and analysis of CFRP propellers and are of great significance to the study of hydrodynamic performance of the propellers.

# References


[1] HONG Y. Structure design and hydroelastic optimiza-

tion of high performance composite propeller [D]. Harbin: Harbin Institute of Technology, 2011 (in Chinese).

[2] LUO H M, HONG Y, WEI K J, et al. The application and study and development of composite propeller [J]. Fiber Composites, 2012 (1): 3−6 (in Chinese).

[3] ZHANG S, ZHU X, SUN H T, et al. Review of researches on composite marine ropellers [J]. Advances in Mechanics, 2012, 42 (5): 620−633 (in Chinese).

[4] ZHANG X T, HONG Y, YUAN F, et al. The development and research of fluid-structure interaction for composite propeller [J]. Fiber Reinforced Plastics/Composites, 2016 (6): 84−87 (in Chinese).

[5] HUANG Z, XIONG Y, YANG G. Composite propeller's strain modal and structural vibration performance [J]. Chinese Journal of Ship Research, 2016, 11 (2): 98−105 (in Chinese).

[6] YAN M J. Research on structural deformation monitoring method based on fiber bragg grating [D]. Nanjing: Nanjing University of Aeronautics and Astronautics, 2015 (in Chinese).

[7] ZETTERLIND III V E, WATKINS S E, SPOLTMAN M W. Feasibility study of embedded fiber optic strain sensing for composite propeller blades [C] // SPIE's 8th Annual International Symposium on Smart Structures and Materials. Newport Beach, CA, United States: SPIE, 2001, 4332: 143−152.

[8] ZETTERLIND V E, WATKINS S E, SPOLTMAN M W. Fatigue testing of a composite propeller blade using fiber-optic strain sensors [J]. IEEE Sensors Journal, 2003, 3 (4): 393−399.

[9] WOZNIAK C D. Analysis, fabrication, and testing of a composite bladed propeller for a naval academy yard patrol (YP) craft [R]. Annapolis: Naval Academy, 2005.

[10] HERATH M T, PRUSTY B G, YEOH G H, et al. Development of a shape-adaptive composite propeller using bend-twist coupling characteristics of composites [C] // Proceedings of the Third International Symposium on Marine Propulsors. Tasmania, Australia: ISMP, 2013: 128−135.

[11] JAVDANI S, FABIAN M, AMS M, et al. Fiber bragg grating-based system for 2-D analysis of vibrational modes of a steel propeller blade [J]. Journal of Lightwave Technology, 2014, 32 (23): 3991−3997.

[12] JAVDANI S, FABIAN M, CARLTON J S, et al. Underwater free-vibration analysis of full-scale marine propeller using a fiber bragg grating-based sensor system [J]. IEEE Sensors Journal, 2016, 16 (4): 946−953.

# 预埋光纤光栅传感器的碳纤维复合材料螺旋桨水下动应变在线测试

雷智洋[1,2], 王春旭[1,2], 吴崇建[1,2], 丁国平[*3], 严小雨[3]

1 中国舰船研究设计中心，湖北 武汉 430064

2 船舶振动噪声重点实验室，湖北 武汉 430064

3 武汉理工大学 机电工程学院，湖北 武汉 430070

**摘　要：**［**目的**］碳纤维复合材料（CFRP）螺旋桨具有轻质高强、低振动、低噪音、耐腐蚀、抗疲劳等优势。为了准确获知CFRP螺旋桨桨叶在水动力载荷下的变形和应变，提出一种水下运转状态下CFRP螺旋桨动应变在线测试方法。［**方法**］将光纤光栅（FBG）传感器预埋于CFRP螺旋桨，搭建CFRP螺旋桨水下动应变测试系统，设置2类测试工况：进速为0 m/s，转速从50~400 r/min依次增加；转速保持427 r/min不变，进速从0~1.6 m/s依次增加。通过FBG传感器采集上述2类工况下CFRP螺旋桨的动应变数据，对动应变数据进行时域和频谱分析。［**结果**］结果表明，CFRP螺旋桨上各测点的动应变特征频率一致，且与转速相关；各测点的动应变峰值取决于测点位置，即螺旋桨的结构力学特征。［**结论**］实现了CFRP螺旋桨在水下运转状态下的动应变在线测试，测试结果合理可靠，可为CFRP螺旋桨的理论设计和分析提供重要的实证依据，对研究螺旋桨振动噪声和水动力性能具有重要意义。

**关键词：**预埋光纤光栅传感器；碳纤维复合材料螺旋桨；动应变；水下在线测试